Cancer Genes and Networks

Molecular Cancer Research

Identification of Genes Regulating Breast Cancer Dormancy in 3D Bone Endosteal Niche Cultures

Julie McGrath[1], Louis Panzica[2], Ryan Ransom[3], Henry G. Withers[4], and Irwin H. Gelman[4]

Abstract

Tumor cell dormancy is a significant clinical problem in breast cancer. We used a three-dimensional (3D) *in vitro* model of the endosteal bone niche (EN), consisting of endothelial, bone marrow stromal cells, and fetal osteoblasts in a 3D collagen matrix (GELFOAM), to identify genes required for dormancy. Human triple-negative MDA-MB-231 breast cancer cells, but not the bone-tropic metastatic variant, BoM1833, established dormancy in 3D-EN cultures in a p38-MAPK–dependent manner, whereas both cell types proliferated on two-dimensional (2D) plastic or in 3D collagen alone. "Dormancy-reactivation suppressor genes" (DRSG) were identified using a genomic short hairpin RNA (shRNA) screen in MDA-MB-231 cells for gene knockdowns that induced proliferation in the 3D-EN. DRSG candidates enriched for genes controlling stem cell biology, neurogenesis, MYC targets, ribosomal structure, and translational control. Several potential DRSG were confirmed using independent shRNAs, including *BHLHE41*, *HBP1*, and *WNT3*. Overexpression of the WNT3/a antagonists secreted frizzled-related protein 2 or 4 (SFRP2/4) and induced MDA-MB-231 proliferation in the EN. In contrast, overexpression of SFRP3, known not to antagonize WNT3/a, did not induce proliferation. Decreased *WNT3* or *BHLHE41* expression was found in clinical breast cancer metastases compared with primary-site lesions, and the loss of *WNT3* or *BHLHE41* or gain of *SFRP1*, *2*, and *4* in the context of *TP53* loss/mutation correlated with decreased progression-free and overall survival.

Implications: These data describe several novel, potentially targetable pathways controlling breast cancer dormancy in the EN.

Introduction

The progression of breast cancer at metastatic sites continues to be the largest contributor to patient mortality (1, 2). There has been renewed focus on identifying the mechanisms governing the establishment of dormancy in specific peripheral sites and the reawakening of dormant cells as major contributors of this cancer's lethal phenotype (3), especially because only a fraction of disseminated tumor cells, and even fewer circulating tumor cells, give rise to clinical macrometastases (4–6). Both estrogen receptor (ER)-positive and triple-negative breast cancers (TNBC: $ER^-/PR^-/Her2^-$) metastasize to and enter dormancy in the bone, with ER^+ tumors often exhibiting a longer-lasting dormancy (7). Importantly, dormant versus active growth depends on which bone niche is colonized (8). Colonization of the endosteal niche (EN), enriched in osteoblasts and marked by low oxygen and high calcium levels, results in dormancy, whereas colonization of the perivascular niche, enriched in hematopoietic stem cells, results in active proliferation and formation of macrometastases (7, 9). Signaling pathways in tumor cells define whether disseminated tumor cells will remain dormant or become proliferative: activation of the p38 MAPK pathway in the absence of ERK1/2 MAPK activity favors quiescence (10). In addition, long-term survival of dormant cells is likely to require adoption of stem-like quiescence properties through increased activity of lineage plasticity pathways. Although several groups identified genes and pathways differentially regulated in dormant versus proliferating breast cancer metastatic cells (8, 11–16), few studies have addressed possible causative roles for these genes, especially in the context of p38 control (16, 17), confounding attempts at therapeutic targeting.

Using a novel 3D-EN culture system developed by Marlow and colleagues (18), in which otherwise aggressive MDA-MB-231 human breast cancer cells become dormant for up to 60 days due to direct contact with EN environmental cells, we show here that the knockdown of p38-MAPK induced proliferation, confirming the notion that dormancy is p38-dependent. To identify genes that promote or maintain dormancy, we used a high-stringency genomic short hairpin RNA (shRNA) screen to identify gene knockdowns that induced proliferation of MDA-MB-231 in 3D-EN cultures. Identification of the top hits, *BHLHE41*, a known p38 target required for induction of quiescence (19), and *LSP1*, a suppressor of ERK1/2 activity (20) increased confidence in the screen's validity. Other gene hits grouped into several regulatory categories not previously identified as suppressors of dormancy. These include genes involved in neurogenesis, translation, and noncanonical WNT signaling, all of which play roles in regulating the maintenance of cancer stem cells. These data strengthen the notion that breast cancer dormancy in the EN is promoted by p38-MAPK–controlled stem cell pathways.

[1]Department of Cancer Biology, University of Arizona, Tucson, Arizona. [2]University at Buffalo School of Law, Buffalo, New York. [3]SUNY Potsdam, Hogansburg, New York. [4]Department of Cancer Genetics and Genomics, Roswell Park Comprehensive Cancer Center, Buffalo, New York.

Note: Supplementary data for this article are available at Molecular Cancer Research Online (http://mcr.aacrjournals.org/).

J. McGrath and L. Panzica are the co-first authors of this article.

Corresponding Author: Irwin H. Gelman, Roswell Park Comprehensive Cancer Center, Elm and Carlton Streets, Buffalo, NY 14263. Phone: 716-845-7681; Fax: 716-845-1698; E-mail: irwin.gelman@roswellpark.org

doi: 10.1158/1541-7786.MCR-18-0956

Materials and Methods

Cell culture

MDA-MB-231 (ATCC HTB-26), MDA-MB-231 BoM1833 (gift from Joan Massague, Memorial Sloan Kettering Cancer Center; ref. 21), HEK293T (ATCC CRL-11268), Phoenix 293T (ATCC CRL-3213), and HS-5 (ATCC CRL-11882) were cultured in DMEM supplemented with 10% FBS and 1% penicillin–streptomycin and incubated at 37°C and 5% CO_2. Human fetal osteoblasts (hFOB; ATCC CRL-11372) were cultured with DMEM/F12 (1:1) media without phenol red and supplemented with 15% FBS and G418 (0.3 mg/mL) and incubated at 32°C and 5% CO_2. Human umbilical vein endothelial cell (HUVEC; Lonza C2517A) were cultured to no more than five passages with EBM-2 media (Lonza CC-3156) supplemented with a SingleQuot pack (Lonza CC-4176) and grown at 37°C and 5% CO_2.

Three-dimensional cultures

Three-dimensional (3D) cultures recapitulating growth in the EN or control 3D collagen matrix growth were produced as described previously (18). Briefly, GELFOAM (Pfizer) discs were cut (5-mm diameter and 3-mm thickness) using a sterile hole punch and scalpel and then UV treated for 2 hours (1.2×10^5 μ J/CM^2) using a UV cross linker. GELFOAM discs were placed into a low attachment 96-well plate (Eppendorf Microplate 96/F-PP, Sigma-Aldrich #C150179G) using sterile forceps. Discs were incubated in 200 μL of 1× Dulbecco PBS at 37°C/5% CO_2 for 20 minutes. EN cultures were produced by seeding HS-5, hFOB, and HUVECs onto GELFOAM discs (4×10^4 cells/5 μL each) via capillary action, incubating for 2 hours, and then topped off with 200-μL niche media. After 24 hours, media were removed and MDA-MB-231 cells (transduced with RFP-expressing shRNA libraries) were seeded onto EN cultures (10^4 cells/10 μL) and grown for 7 days, with niche media (100 μL) replaced daily. MDA-MB-231 cells grown on tissue culture plates (2D) or in GELFOAM alone (3D) served as negative controls. Bone-tropic MDA-MB-231 (BoM1833) cells, infected with pGIPZ (GFP-expressing) lentivirus vector, served as a positive control for 3D-EN growth. MDA-MB-231 growth was monitored every other day via fluorescence microscopy using a Nikon Eclipse TS100 inverted microscope and SPOT Insight Fire Wire Camera and SPOT 5.2 software. Cell numbers were quantified using ImageJ software (NIH) from five different fields containing >100 cells/field.

shRNA and expression vectors

Lentivirus shRNA clones (pGIPZ-based; Supplementary Table S2), Cellecta Human DECIPHER RFP screening libraries (Table 1), and DNA expression vectors (ORFeome 8.1) were provided by the Roswell Park Comprehensive Cancer Center Gene Modulation Core (I.H. Gelman, Director). Plasmids were propagated in *Stbl3* bacteria (Thermo Fisher Scientific) in LB media supplemented with 100 μg/mL ampicillin for 18 hours at 37°C at a constant speed of 200 rpm. Plasmids were extracted using QIAprep Spin Miniprep Kit (Qiagen catalog no. 27104) according to the manufacturer's protocol. Relative plasmid concentrations were quantified using a Nanodrop 2000 (Thermo Fisher Scientific).

Transfection

HEK293T cells were transfected with LipoD293/DNA mixtures as described previously (22).

Lentivirus packaging and infection

Polytropic lentiviruses were packaged in HEK293T cells using psPAX2 and pMD2.G packaging constructs as described previously (23). For infection of target cells plated the previous day at confluency in 6-well dishes, 150 μL of lentiviral supernatant and 4 μg/mL polybrene (Sigma) was added to the cells along with 1–2 mL DMEM (10% FBS, 1% penicillin/streptomycin) until cells were completely covered. Cells were then incubated for 30 minutes at 37°C with 5% CO_2, centrifuged at 1,800 rpm for 45 minutes, and then incubated overnight again at 37°C/5% CO_2. The cultures were split at a 1:5 ratio in DMEM containing 10% FBS, 1% penicillin/streptomycin, 2 mg/mL puromycin.

PCR

RNA was extracted using TRIzol (Life Technologies) according to the manufacturer's protocol. One microgram of total RNA/reaction was used in qRT-PCR reactions (50 μL total volume) containing High Capacity cDNA Reverse Transcriptase Kit reagents (Life Technologies/Applied Biosystems #4368814). qPCR was performed using Power SYBR green PCR Mastermix (Life Technologies #4367659) on a Step One Plus thermocycler (Applied Biosystems). *GAPDH* housekeeping gene was used as the loading control. qRT-PCR reactions were performed in triplicate and relative concentrations were determined using the $2^{-\Delta\Delta C_t}$ method (StepOne software).

Immunoblot analysis

Immunoblot analysis was performed, as described previously (24), using the following antibodies: primary—V5 tag (Thermo Fisher Scientific, #37-7500), GAPDH (Santa Cruz Biotechnology, #sc-25778), α-tubulin (Santa Cruz Biotechnology, #sc-5286), p38-MAPK (Cell Signaling Technology, #9212), $p38^{poT180/Y182}$ (Cell Signaling Technology, #9211), ERK1/2 (Cell Signaling Technology, #9102S), $ERK1/2^{poT202/Y204}$ (Cell Signaling Technology, #9101S); secondary—Alexa Fluor700 anti-mouse Ig (1:1,000) or Alexa Fluor800 anti-rabbit Ig (1:10,000).

Table 1. shRNA library and screening criteria

Human module	Gene targets	# of target mRNAs	shRNA complexity
1	Signaling pathway targets	5,043	27,500
2	Disease-associated targets	5,412	27,500
3	Cell surface, extracellular, DNA-binding targets	4,922	27,500
Hit criteria	**Definition**	**Module #**	**# of hits**
Fold increase	≥1.55	1	65
# clones	≥3	2	139
Replicates	≥2 of 3	3	198
p38 regulated	Up- or down-regulated		
Metastasis	Involved?		

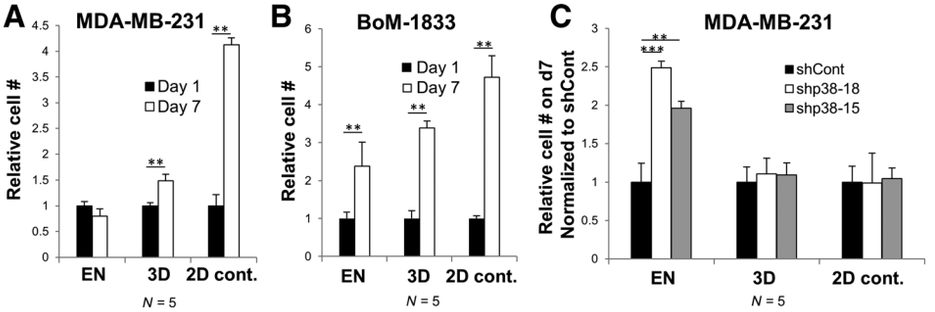

Figure 1.
Dormancy induction in 3D-EN is p38-MAPK–dependent. Relative cell numbers of MDA-MB-231 (**A**), MDA-MB-231[BoM1833] (**B**), or MDA-MB-231 cells with p38 knockdown (vs. shCont.; **C**) grown for either 1 or 7 days in 3D-EN or 3D, or in 2D (control) conditions ($N =$ independent replicates; error bars, SEM; **, $P < 0.001$).

High-throughput sequencing and gene identification

DNA was isolated from 7-day 2D and 3D-EN cultures using phenol/chloroform/isoamyl (25:24:1). Cells in the 3D culture were isolated by removing GELFOAM discs with cells and incubating on a rotator for 1 hour at 37°C in 5 mL 1× collagenase/hyaluronidase solution (STEMCELL Technologies). After vigorous mixing, cells were pelleted and washed three times with PBS. First-round and nested PCR were performed according to the Cellecta shRNA library manual (http://www.cellecta.com/resources/product-manuals-and-certificates/), as we described previously (23) using primers described in Supplementary Table S3. All experiments were conducted in triplicate. The PCR products were cleaned using QIAquick Gel Extraction Kits, and then subjected to single-end rapid mode sequencing on an Illumina HiSeq2500 as performed by the Roswell Park Comprehensive Cancer Center Genomics Shared Resource (Sean Glenn, Director). Using FASTQ sequencing data files, barcodes were trimmed from flanking sequence using the *ShortRead* package from Bioconductor (25). The isolated barcode sequences were aligned to a reference file matching shRNA clones to gene targets using the DECIPHER BarCode Deconvoluter program (Cellecta), which allows for up to two incorrect base changes for accurate barcode identification. Individual sequence read counts were normalized by total reads sequenced, and top hits were filtered on the basis of a threshold determined by luciferase shRNA-negative controls (16 clones). An analysis of row sums was performed to identify genes targeted by multiple shRNA clones and across replicates.

Statistical analysis

Statistical analysis was performed on the fold-change between the cell counts from day 1 to 7 using the Student two-tailed *t* test. Error bars indicate SEM. Significant differences between experimental groups had a *P* value lower than 0.05.

Results and Discussion

Using a novel 3D model of dormancy for bone-metastatic breast cancer (18), we endeavored to identify genes that suppress tumor cell quiescence in a cultured microenvironment recapitulating bone EN. In this model, the human TNBC cell line MDA-MB-231 proliferates in a GELFOAM biomatrix, whereas it is growth-arrested in EN conditions (hFOBSs, HUVECs, and HS-5 diploid fibroblasts in GELFOAM; Fig. 1A). Importantly, the inclusion of bone marrow origin fibroblasts (HS-5) and human endothelial cells (HUVEC) promoted the long-term survival of hFOB osteoblasts even after these cells reached initial confluence after 24 hours of growth. This EN culture condition was previously shown to induce growth arrest of ER-positive (MCF7, T47D, ZR75-1, and BT474) and ER-negative (SUM149, SUM159, MDA-MB-231, and MDA-MB-453) human breast cancer cell lines, whereas these lines could proliferate in either GELFOAM alone, or in GELFOAM seeded with primary human bone marrow stem cells, representing a perivascular niche (18). In contrast, the bone-metastatic MDA-MB-231 variant, BoM1833, which was selected *in vivo* for increased bone growth (26), proliferates in either niche (Fig. 1B). Consistent with the notion that activated p38 MAPK in the absence of MEK-ERK activation favors dormancy, we showed that the knockdown of p38 by shRNA (shRNA clones #15 and #18) also induced MDA-MB-231 proliferation in the EN (Fig. 1C), consistent with previous data (18) using the p38 kinase inhibitor, SB203580.

To identify the suppressors of tumor cell proliferation in a bone niche, MDA-MB-231 cells were transduced with a genomic shRNA library (Cellecta DECIPHER library covering 15,377 human genes with 82,500 independent shRNA clones, divided into 3 modules; Table 1) and clones that proliferated in EN cultures were enriched. Genes that are potentially required for MDA-MB-231 dormancy within the EN were identified by performing next-generation sequencing of shRNA clone barcodes from DNA taken from triplicate screen aliquots of freshly infected cells (24 hours) and from infected cells incubated for 7 days in 3D-EN. The barcode sequences were trimmed from flanking sequences and shRNA-targeted genes then identified using Cellecta's BarCode Deconvoluter software. We selected gene targets (shRNA barcodes) that were found in $\geq$2 of three independent screens, identified by $\geq$3 independent shRNA clones/gene, each at >1.5-fold increase over background (normalized against the relative abundance of each clone in the library; Table 1). This analysis identified 416 potential "dormancy-reactivation suppressor" genes (DRSG) in the 3 shRNA clone modules (Table 1).

One of the ways we established statistical significance for potential DSRG candidates was to compare the relative frequency of shRNA clones with the 16 luciferase shRNA controls (shLuc) contained within each module. For example, 2 module-2 genes, *DOLK* and *MICALL2*, had at least 2 independent shRNA clones with fold-change sequence reads over the 1.55-fold shLuc

Table 2. DSRG candidates subjected to secondary validation

Gene targets	Human module	Fold increase in proliferation at d7	*P*
MAPK14	–	2.4 ± 0.4	<0.001
HBP1	1	1.8 ± 0.16	<0.01
WNT3	1	2.9 ± 0.4	<0.001
NES	1	0.9 ± 0.2	N.S.
BHLHE41	1	2.2 ± 0.2	<0.001
TIAL1	2	1.1 ± 0.2	N.S.
HTATIP2	2	1.06 ± 0.032	N.S.
DOLK	2	1.04 ± 0.06	N.S.

Table 3. Module-1 DSRG candidates

Gene	Fold increase*	# Of hits	p38-Related**	Metastasis	Pathway
ADCY8	1.81	5	No	no	Neuro/stem
ADK	1.90	4	No	no	Neuro/stem
ADRB2	2.19	5	Yes	Yes	Neuro/stem
ARG1	1.64	4	No	No	Neuro/stem
ATG2A	2.00	4	No	No	Autophagy
ATP2B1	1.91	4	No	No	Ca transport
BHLHE41[a]	2.3	5	Yes	Yes	p38/dormancy
BIK	1.56	4	No	Yes	Apoptosis
BRD4	1.78	7	No	Yes	Neuro/stem
CACNA1B	1.75	4	No	No	Neuro/stem
CACNB3	2.70	5	Yes	No	Neuro/stem
CASR	1.76	5	Yes	Yes	Neuro/stem
CD63	1.62	4	Yes	Yes	β-catenin signal
CDC2L1	1.84	5	Yes	Yes	Translation
CFD	2.23	5	No	No	?
CHRND	1.80	4	No	No	Neuro/stem
CIP29	2.31	6	No	No	Translation
CLDN2	1.88	4	No	Yes	Neuro/stem
CLK3	1.64	4	No	No	Translation
EHF/ESE3	2.33	4	Yes	No	Neuro/stem
EIF2S3	2.45	4	No	No	Translation
EIF4A1	1.82	4	No	Yes	Translation
EME2	1.71	5	No	No	DNA repair
F10	1.68	4	No	No	Coagulation
FLT1 (VEGFR1)	1.74	4	Yes	Yes	Met. promoter
FUBP1	2.39	6	No	Yes	Translation
GABRG3	1.70	5	No	No	Neuro/stem
GCGR	1.60	4	No	No	Neuro/stem
GFPT2	1.82	5	No	No	Metabolism
GHRL	1.70	4	No	No	Metabolism
GPD2	1.85	4	No	No	Metabolism
HBP1[a]	1.85	5	Yes	Yes	Neuro/stem
HMGB2	1.84	4	No	No	Neuro/stem
HSPD1	1.71	4	No	Yes	Chaperone
IL2RG	1.84	4	No	No	Survival
IREB2	1.60	4	No	No	Iron metabolism
KEAP1	2.26	5	Yes	Yes	Neuro/stem
KIF11	2.22	11	No	Yes	Met. promoter
KREMEN1	1.69	5	No	No	Survival
LSP1	2.20	5	Yes	Yes	ERK1/2 supp
NEDD8	1.81	4	No	No	Neuro/stem
NES	1.76	5	No	Yes	Neuro/stem
NNAT	2.63	7	Yes	No	Neuro/stem
NOB1	2.67	6	Yes	Yes	Translation
NOX1	1.86	7	No	Yes	Neuro/stem
NRG1	1.97	4	Yes	Yes	Neuro/stem
OASL	2.84	3	Yes	No	Translation
OGG1	1.85	6	No	No	DNA repair
P11 (s100A10)	1.79	4	Yes	Yes	Breast cancer adhesion
PDE6H	1.91	4	No	No	cAMP metabol
PLLP	2.20	4	No	No	Metabolism
PSMB4	2.03	4	No	No	Neuro/stem
PSMC6	2.29	4	No	No	Neuro/stem
PSMD7	1.68	6	No	No	Neuro/stem
RELN	1.96	4	No	Yes	Neuro/stem
SCN7A	1.63	4	No	No	Na channel
SERPIN1	1.55	4	No	Yes	Invasion
SHC3	2.02	6	No	No	Neuro/stem
SUOX	1.98	4	No	No	Metabolism
TAC4	2.27	7	Yes	No	Neuro/stem
TTF1	2.26	5	Yes	Yes	Neuro/stem
VARS	2.02	5	No	No	Translation
WNT3[a]	1.91	5	Yes	Yes	β-catenin signal
WNT8A	2.23	4	No	Yes	β-catenin signal
YARS	1.62	4	No	No	Translation

[a]Confirmed by independent shRNA knockdown.

*Fold increase in 7-day vs. 1-day growth in 3D-EN, in triplicate samples.

**Pubmed evidence as either a p38 substrate, expression regulated by p38 or modulation of p38 expression or activity.

Table 4. Translation-controlling potential DSRG

Gene	Gene name	Function
60S Subunit		
RPL3	Ribosomal protein L3	Ribosome, structural
RPL4	Ribosomal protein L4	Ribosome, structural
RPL6	Ribosomal protein L6	Ribosome, structural
RPL7	Ribosomal protein L7	Ribosome, structural
RPL8	Ribosomal protein L8	Ribosome, structural
RPL10	Ribosomal protein L10	Ribosome, structural
RPL12	Ribosomal protein L12	Ribosome, structural
RPL13A	Ribosomal protein L13A	Ribosome, structural
RPL14	Ribosomal protein L14	Ribosome, structural
RPL21	Ribosomal protein L21	Ribosome, structural
RPL23	Ribosomal protein L23	Ribosome, structural
RSL24	Ribosomal protein L24	Ribosome, structural
RPL32	Ribosomal protein L32	Ribosome, structural
RPL37A	Ribosomal protein L37A	Ribosome, structural
40S Subunit		
RPS4X	Ribosomal protein S4X	Ribosome, structural
RPS14	Ribosomal protein S14	Ribosome, structural
RPS15AP17	Ribosomal protein S15a pseudogene 17	
RPS20	Ribosomal protein S20	Ribosome, structural
RPS26	Ribosomal protein S26	Ribosome, structural
RPS27AP5	Ribosomal protein S27a pseudogene 5	
RPL36P14	Ribosomal protein L36 pseudogene 14	
Elongation factors		
EIF2B5	Eukaryotic translation initiation factor 2B subunit ε	Elongation factor
EIF2S2	Eukaryotic translation initiation factor 2B subunit β	Elongation factor
EIF2S3	Eukaryotic translation initiation factor 2B subunit γ	Elongation factor
EIF3A	Eukaryotic translation initiation factor 3 subunit A	Elongation factor
EIF4A1	Eukaryotic translation initiation factor 4A1	Elongation factor
Misc. regulators		
CLK3	CDC-like kinase 3	Regulates splicing factors
FCF1	rRNA-processing protein	Ribosome formation
KARS	Lysyl tRNA synthase	Codon usage
NARS2	Asparaginyl-tRNA synthetase 2	Codon usage
NOB1	NIN1 binding protein 1	rRNA processing
TSFM	Ts translation elongation factor, mitochondrial	Mitochondrial translation
VARS	Valyl-tRNA synthetase	Codon usage
YARS	Tyrosyl-tRNA synthetase	Codon usage

threshold (Supplementary Fig. S1A), yet when compared between screening replicates, only the *MICALL2* clones showed consistent statistical significance over the luciferase clones (Supplementary Fig. S1B) in $\geq$2 replicates. Indeed, the knockdown of *DOLK* using independent shRNAs failed to induce increase MDA-MB-231 proliferation in 3D-EN cultures (Table 2).

Many studies have shown that metastatic dormancy is controlled by the simultaneous upregulation of p38MAPK and downregulation of ERK activation (27), yet little is known about mediators of dormancy downstream of p38MAPK. Thus, DSRG were subjected to Ingenuity Pathway Analysis and PubMed search to bin them based on a predicted or known relationship to p38MAPK signaling and metastasis. An example is shown in Table 3 for the 65 potential DSRGs from module-1, relative to their relationship to p38MAPK signaling and metastasis. Of these candidates, 14 genes were associated with both p38MAPK signaling and metastasis (*ADRB2*, *BHLHE41*, *CASR*, *CD63*, *CDC2L1*, *FLT1*, *HBP1*, *KEAP1*, *LSP1*, *NOB1*, *NRG1*, *P11*, *TTF1*, *WNT3*), 12 genes were associated with metastasis but not with p38MAPK signaling (*BIK*, *BRD4*, *CLDN2*, *EIF4A1*, *FUBP1*, *HSPD1*, *KIF11*, *NES*, *NOX1*, *RELN*, *SERPIN1*, *WNT8A*), and 5 genes were associated with p38MAPK signaling alone (*CACNB3*, *EHF*, *NNAT*, *OASL*, *TAC4*). As a whole, there was a selection for DSRG candidates in module-1 that are involved in the regulation of neurogenesis or stem cell biology (Table 3), and/or protein translation (Tables 3 and 4). Loss of differentiation (neurogenesis) or stem cell induction genes resulting in active breast cancer cell growth in the 3D-EN is consistent with the notion that disseminated tumor cells exhibit stem cell–like properties (28, 29). Differential expression of genes controlling ribosome biogenesis are known to control stem cell homeostasis (30), and indeed, the antagonism of this process was shown to inhibit tumor formation induced by $CD44^{+}/CD24^{-}$ human breast cancer stem cells (31).

In contrast, several gene candidates had roles that might directly control known dormancy functions. For example, *BHLHE41* has been reported to play a role in p38MAPK-mediated dormancy (19), *ADRB2* suppresses prostate cancer proliferation in bones by downregulating osteoblast-expressed GAS6 (32), *LSP1* negatively controls ERK signaling (20), and *P11* (*S110A10*) controls breast cancer adhesion to endothelial cells in the metastatic niche (33). Finally, gene set enrichment analysis of all the module-1 genes showed that 18 of 65 genes (27.7%) were likely MYC targets (Fig. 2A). Although a role of MYC as a driver of dormancy reawakening has not been addressed, MYC amplification is associated with high-grade breast cancer and worse prognosis (34), and in several non-breast cancer models, the forced reexpression of MYC rescues proliferation in dormant tumor cells (35).

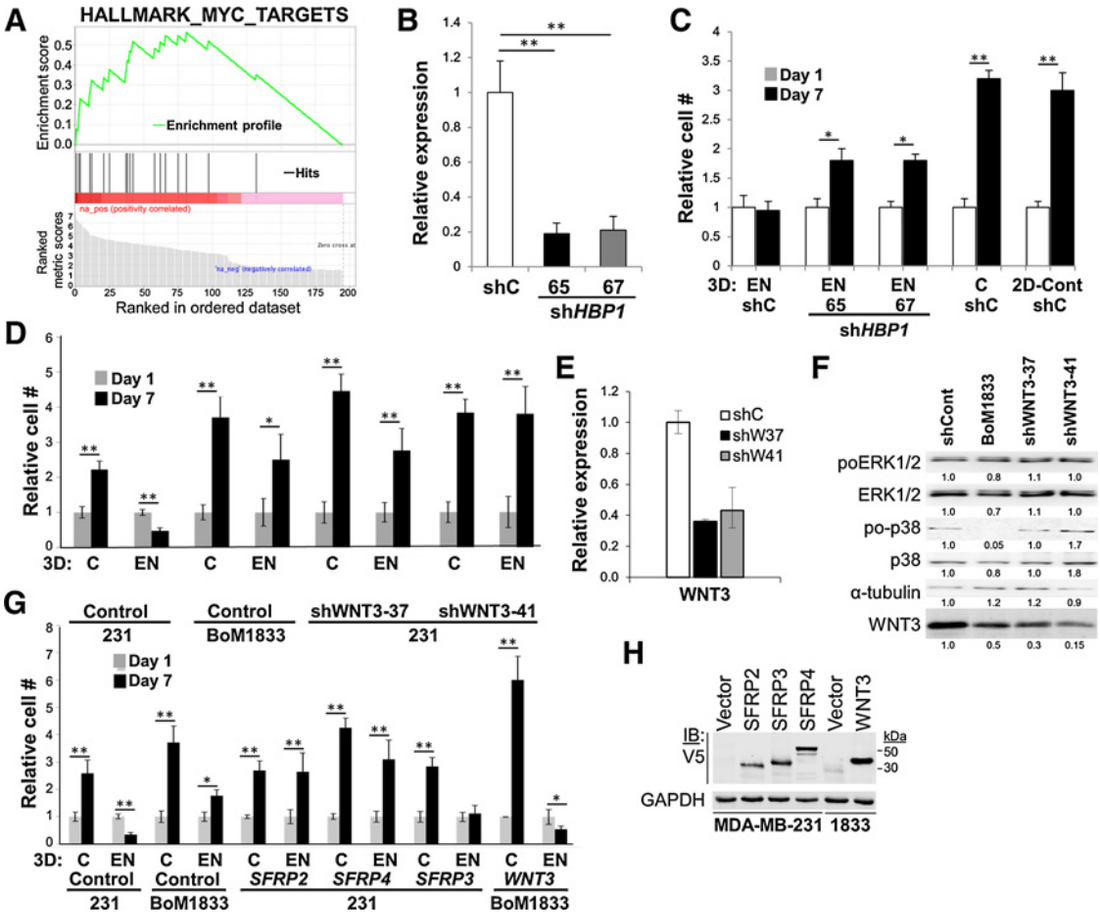

Figure 2.

Analysis of *HBP1* and *WNT3* as potential DSRG. **A,** Gene set enrichment analysis of module-1 DSRG candidates identified 18 of 65 hits as being MYC target genes. **B,** qRT-PCR showing knockdown of *HBP1* in MDA-MB-231 cells. Knockdown of *HBP1* (**C**) or *WNT3* (**D**) induces proliferation in 3D-EN versus 3D ("C") or 2D cultures. Error bars, SEM of three independent replicates; *, $P < 0.01$; **, $P < 0.001$. **E,** Confirmation of *WNT3* knockdown by qRT-PCR. Error bars, SEM of three independent replicates. **F,** Immunoblot of lysates of MDA-MB-231 or BoM1833 transduced with scramble shRNA ("shCont"), or *WNT3*-knockdown MDA-MB-231 cells probed for total or activated (poT202/Y204) ERK1/2, total or activated (poT180/Y182) p38-MAPK or α-tubulin (as a loading control). Digital quantifications are shown as normalized to the shCont. This blot is typical of three independent experiments. **G,** Overexpression of *SFRP2* or *4*, but not *SFRP3*, in MDA-MB-231 induces proliferation in 3D-EN cultures, whereas the overexpression of *WNT3* in BoM1833 suppresses 3D-EN proliferation. Error bars, SEM of three independent replicates; *, $P < 0.01$; **, $P < 0.001$. **H,** Immunoblot of MDA-MB-231 lysates transduced with lentivirus expressing V5-tagged *SFRP2, 3,* or *4* (or empty vector), or BoM1833 ("1833") cells transduced with *WNT3* (or empty vector), probed for V5 or GAPDH. Molecular weight markers are at right.

We then sought to independently confirm that the downregulation of several DSRG candidates leads to MDA-MB-231 proliferation in 3D-EN cultures. Thus, MDA-MB-231 cells were transduced with 2 independent shRNA clones/gene, and following confirmation of gene knockdown by either qRT-PCR or immunoblotting, the cells were assessed for proliferation (vs. scrambled shRNA controls) in 3D-EN cultures as in Fig. 1. For this analysis, we chose three predicted DSRG from module-1, *BHLHE41*, *HBP1*, and *WNT3*, which were both p38- and metastasis-associated (Table 3), and 1 gene, *NES*, not known to be p38-regulated. As well, we chose two negative controls (not predicted to be DSRG): *DOLK*, which was neither p38- nor metastasis-associated (Supplementary Table S1) and that was likely not significant due to lack of replicate hits (Supplementary Fig. S1B), and *HTATIP2*, a module-2 gene that failed to make the cut because it had only 2 shRNA hits in one of three replicates. *BHLHE41*, *HBP1*, and *WNT3* were validated as DSRG, that is, their knockdown resulted in significantly increased proliferation in EN over controls (*BHLHE41:* Table 2, *HBP1* and *WNT3:* Fig. 2C and D), whereas *DOLK*, *NES*, and *HTATIP2* knockdown failed to induce MDA-MB-231 proliferation in the 3D-EN (Table 3).

WNT signaling largely has been linked to metastatic progression, especially in models of TNBC (36). However, recent data suggest that specific WNT family members, such as WNT5A, might promote either metastatic progression or dormancy, depending on whether signaling is through canonical or noncanonical pathways (37). Therefore, we sought to follow-up our finding that WNT3 knockdown induced MDA-MB-231 proliferation in our 3D-EN assay. First, we confirmed that WNT deficiency caused proliferation (Fig. 2D), using two independent WNT3-specific shRNAs, which knocked down the WNT3 expression in MDA-MB-231 cells approximately 2.5-fold over scrambled

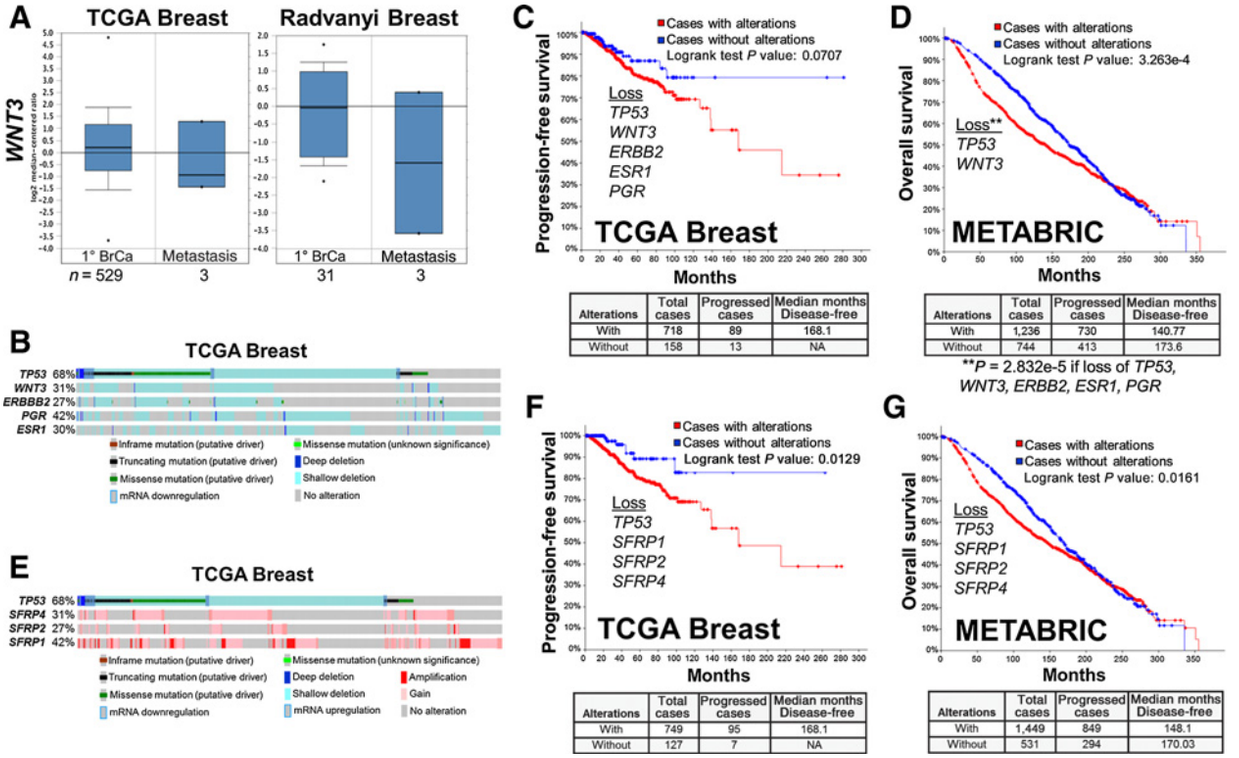

Figure 3.

WNT3 expression in clinical breast cancer (BrCa) datasets and correlation with survival. **A,** Oncomine TCGA Breast and Radvanyi datasets showing relative *WNT3* expression in primary (1°) versus metastatic breast cancer cases. *N* = number of cases. **B,** Copy number variations, mutations, and expression changes of *TP53, WNT3, ERBB2, PGR, and ESR1* in the TCGA Breast dataset produced through cBioPortal, with vertical bars representing a single patient, and the percentages representing the total changes for a given gene. Progression-free (**C**) and overall survival (**D**) for TGCA Breast and METABRIC datasets, respectively, based on combined *TP53, WNT3, ERBB2, PGR, and ESR1* losses in the TGCA data, and *TP53* and *WNT3* losses in the METABRIC dataset. The number of cases with or without these gene changes, as well as the median number of disease-free months, are shown below. **E,** Copy number variations, mutations, and expression changes of *TP53, SFRP1, 2,* and *4* in the TCGA Breast dataset produced through cBioPortal. Progression-free (**F**) and overall survival (**G**) for TGCA Breast and METABRIC datasets, respectively, based on combined *TP53, SFRP1, 2,* and *4* losses, with numbers of cases with or without changes (below).

controls (shCont; Fig. 2E). Interestingly, WNT3 levels were relatively decreased in BoM1833 cells, consistent with the notion that WNT3 loss facilitates proliferation in the 3D-EN (Fig. 2F). However, WNT3 knockdown in MDA-MB-231 cells had no effect on relative p38$^{poT180/Y182}$ levels, indicating that the increased proliferation of MDA-MB-231 cells after WNT3 deficiency was not a result of loss of p38 activation. Although this finding would be consistent with *WNT3* being a downstream mediator of p38 signaling, we cannot rule out that the *WNT3* effect is p38-independent. In contrast, the BoM1833 variant, which failed to growth-arrest in the 3D-EN cultures (Fig. 1B), exhibited decreased relative p38 activation levels.

Secreted forms of frizzled-related proteins (SFRP) are thought to antagonize WNT/β-catenin signaling by directly binding WNT members (38), and more specifically, SFRP2 and 4, but not SFRP3, are known to bind WNT3 at high affinity (39). We therefore transduced MDA-MB-231 cells with V5-epitope tagged SFRP2, 3, or 4 expressing vectors, confirmed ectopic expression versus an empty vector control (Fig. 2H), and tested these cells for proliferation in 3D-EN cultures. Figure 2G shows that SFRP2 and 4, but not 3, could release MDA-MB-231 cells from dormancy. Similarly, the overexpression of WNT3 in BoM1833 suppressed proliferation in 3D-EN, but not in 3D-control cultures (Fig. 2G). Taken together, these data strongly suggest that WNT3 promotes dormancy in our 3D-EN model. This is consistent with a report showing that increased Hedgehog-mediated Sfrp1 expression in liver stroma increased the metastatic potential of human Capan-1 pancreatic tumor cells through the suppression of WNT3 signaling, and that the overexpression of WNT3A in Capan-1 cells decreased experimental metastasis formation (40).

To address this in a clinical context, we compared the relative *WNT3* expression levels in primary-site versus metastatic breast cancers in The Cancer Genome Atlas (TCGA) and Radvanyi Oncomine datasets (41). These data show lower levels of *WNT3* in clinical macrometastases compared with primary-site breast cancer (Fig. 3A), suggesting that *WNT3* deficiency promotes active metastatic progression. One drawback, however, is that both studies have very few metastatic cases (three each), with none derived from bone, confounding the determination of statistical significance. We then analyzed how the loss of *WNT3* correlates with either progression-free or overall survival using the TCGA Breast and METABRIC (42, 43) datasets in cBioPortal (http://www.cbioportal.org). We noted that *WNT3* loss, either due to gene deletion or transcriptional downregulation, occurred in 31% and 21% of all breast cancer cases in TCGA and METABRIC, respectively, and that these cases showed strong cooccurrence

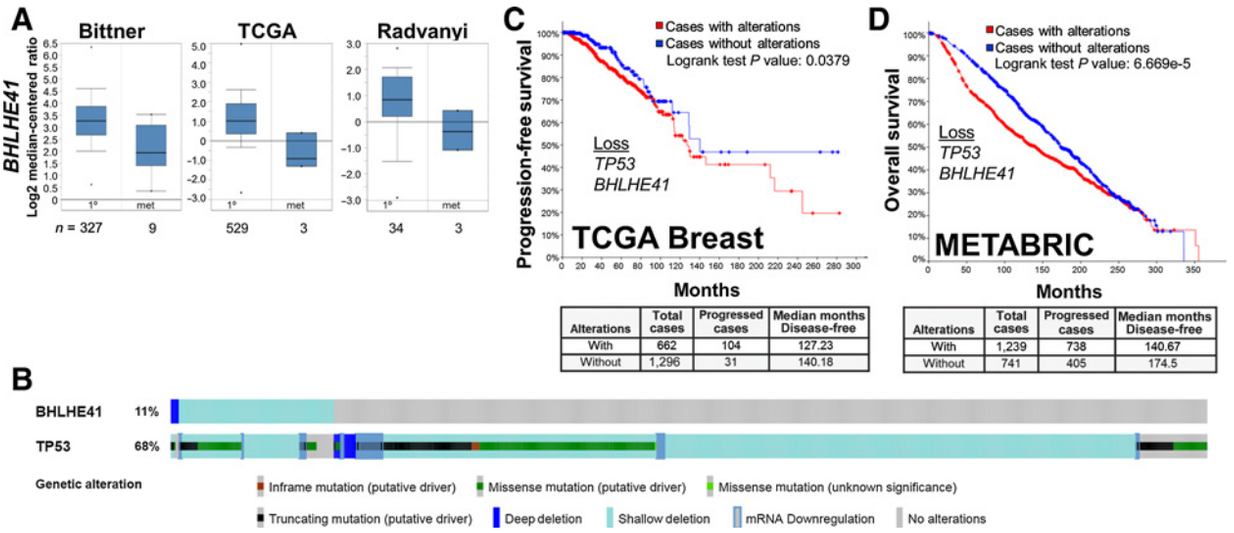

Figure 4.

BHLHE41 expression in clinical breast cancer datasets and correlation with survival. **A,** Oncomine Bittner, TCGA Breast, and Radvanyi datasets showing relative *BHLHE41* expression in primary (1°) versus metastatic breast cancer cases. *N* = number of cases. **B,** Copy number variations, mutations, and expression changes of *TP53* and *BHLHE41* in the TCGA Breast dataset produced through cBioPortal, with vertical bars representing a single patient, and the percentages representing the total changes for a given gene. Progression-free (**C**) and overall survival (**D**) for TGCA Breast and METABRIC datasets, respectively, based on combined *TP53* and *BHLHE41* losses in the METABRIC dataset. The number of cases with or without these gene changes, as well as the median number of disease-free months, are shown below.

with the loss/mutation of *TP53* (*P* values of 1.36e-21 and 2.98e-58, respectively). Indeed, clinical cases of TNBC are marked by specific *TP53* mutations (44). We then sought to determine whether the loss of *WNT3* and/or *TP53* predicted poorer clinical survival, or whether any survival correlation associated with *WNT3* loss was potentiated in a background of ER, progesterone receptor (PR) and HER2 loss (encoded by *ESR1*, *PGR*, and *ERBB2*, respectively), reflecting TNBC. Indeed, a large portion of the WNT3-deficient cases in the TCGA breast dataset had coincident losses of *ESR1*, *PGR*, and *ERBB2* (Fig. 3B). Figure 3C shows that in the TCGA dataset, poorer progression-free survival was only detected in cases with combined losses of *WNT3*, *TP53*, *ESR1*, *PGR*, and *ERBB2*; the loss of any of these genes alone or the combined loss of *ESR1*, *PGR*, and *ERBB2* did not affect survival (*WNT3* loss alone: $P = 0.652$; *TP53* loss alone: $P = 0.125$; *WNT3* plus *TP53* loss: $P = 0.0855$; ESR1, *PGR*, and *ERBB2* combined loss: $P = 0.300$). It is noteworthy that BRCA1 mutational status, which represents fewer than 3% of all the *WNT3*-deficient cases in the TGCA Breast database, has no effect on survival (*WNT3* loss + *BRCA1* mutation: $P = 0.693$). In contrast, loss of only *WNT3* and *TP53* in the METABRIC dataset showed poorer survival (Fig. 3D). Taken together, these data show that *WNT3* loss contributes to poorer survival, especially in the context of *TP53* loss. The superior powering of the METABRIC dataset, and the fact that it includes many more cases of disease recurrence/progression associated with metastasis, allows for the conclusion that *WNT3*/*TP53* loss is sufficient for poorer survival, a value that worsens in the context of what are likely triple-negative cases (*ESR1*, *PGR*, and *ERBB2* loss). These data correlate with the fact that TNBC dormancy in the bones is shorter in duration than that of ER-positive breast cancer (7), suggesting that the combined loss of ER, PR, and HER2 might sensitize dormant breast cancer cells toward *WNT3* loss. It is important to note that we only studied the role of WNT3 signaling in tumor cells in the context of a 3D-EN microenvironment. Although secreted factors are likely to play an important role, it should be noted that cell–cell contact was required for MDA-MB-231 dormancy in this 3D-EN (18). The exact roles played by each EN niche cell type, whether in its direct interaction to breast cancer cells or through its secretome, remains to be elucidated. In addition, the role of WNT3 in controlling tumor dormancy in the bone may be cancer type–dependent because Nandana and colleagues (45) showed that prostate cancer invasiveness and bone colonization required TBX2-regulated WNT3A expression.

We performed a similar analysis on the two other validated DSRG, which indicated that *BHLHE41*, but not *HBP1*, exhibited decreased expression in breast cancer metastases compared to levels in primary tumors (Fig. 4A; Supplementary Fig. S1C). In the TCGA Breast dataset, 11% of cases exhibited partial or full loss of *BHLHE41* (Fig. 4B). As with *WNT3* loss, the loss of *BHLHE41* had a statistical cooccurrence with mutation/loss of *TP53* ($q = 0.0242$) in this dataset. Moreover, the combined loss of *BHLHE41* and *TP53* correlated with decreased progression-free or overall survival, respectively, in the TCGA Breast and METABRIC datasets (TCGA: $P = 0.0379$; METABRIC: $P = 6.669\text{e-}5$). In contrast, loss of *BHLHE41* alone did not correlate with decreased survival in TCGA Breast ($P = 0.568$). Interestingly, the combined loss of *WNT3*, *BHLHE41*, and *TP53* did significantly change the rate of progression-free survival in TCGA Breast cases, strongly suggesting that the *WNT3*/*TP53* and *BHLHE41*/*TP53* loss cohorts were independent groups, and that either loss of *WNT3* or *BHLHE41* was individually capable of initiating reawakening in the context of *TP53* loss. This also suggests that *TP53* loss is the main driver of the poorer prognosis. In regards to possible mechanisms underlying *BHLHE41* as a DSRG, the gene product, BHLHE41 (also known as DEC2 and SHARP1), functions as a transcriptional repressor of

epithelial-to-mesenchymal transition and invasion factors, SNAI1, SNAI2, and TWIST (46). In addition, Adorno and colleagues (47) showed that breast cancer cases with higher levels of *BHLHE41* and *CCNG2*, two p63-induced genes, correlated with lower metastatic risk. Interestingly, specific sets of p53 mutations abrogate p63 activity, likely leading to *BHLHE41* loss (48).

In conclusion, this study marks a novel method to identify and validate potential DSRG based on an *in vitro* 3D-EN dormancy model for breast cancer. Our data suggest several therapeutic avenues, but these would likely be divided into treatments that either secure dormancy, that is, antagonize reawakening, or that induce large-scale reawakening in a neoadjuvant setting, linked to standard chemotherapies prescribed for TNBC. Examples of reawakening suppressors might include small-molecule inhibitors of MYC (49) or Nutlin-3a to normalize mutant p53 function (50), whereas inducers of reawakening might include inhibitors of WNT3 signaling (51, 52) or p38 kinase activity (53).

Disclosure of Potential Conflicts of Interest

I.H. Gelman is a consultant/advisory board member for Gerson Lehman Group and Kinex LLC (now Athenex Inc.). No potential conflicts of interest were disclosed by the other authors.

Authors' Contributions

Conception and design: I.H. Gelman
Development of methodology: J.E. McGrath, R. Ransom
Acquisition of data (provided animals, acquired and managed patients, provided facilities, etc.): J.E. McGrath, L. Panzica, H.G. Withers
Analysis and interpretation of data (e.g., statistical analysis, biostatistics, computational analysis): J.E. McGrath, L. Panzica, H.G. Withers
Writing, review, and/or revision of the manuscript: L. Panzica, H.G. Withers, I.H. Gelman
Administrative, technical, or material support (i.e., reporting or organizing data, constructing databases): L. Panzica, H.G. Withers
Study supervision: I.H. Gelman

Acknowledgments

The authors thank G. Dontu for critical discussion regarding the 3D bone growth models. This work was supported by the Roswell Park Alliance Foundation and by NCI grant P30-CA016056 involving the use of Roswell Park Comprehensive Cancer Center's Genomics, Bioinformatics, and Gene Modulation Shared Resource. This work was also supported by grant CA94108 (NIH/NCI) and by an Alliance Foundation grant (to I.H. Gelman), and in part, through NCI Comprehensive Cancer funds (P30-CA016056) involving the use of Roswell Park Comprehensive Cancer Center's Genomics and Gene Modulation Shared Resources.

The costs of publication of this article were defrayed in part by the payment of page charges. This article must therefore be hereby marked *advertisement* in accordance with 18 U.S.C. Section 1734 solely to indicate this fact.

Received September 7, 2018; revised October 17, 2018; accepted January 7, 2019; published first January 16, 2019.

References

1. Zhang XH, Giuliano M, Trivedi MV, Schiff R, Osborne CK. Metastasis dormancy in estrogen receptor-positive breast cancer. Clin Cancer Res 2013;19:6389–97.
2. Banys M, Hartkopf AD, Krawczyk N, Kaiser T, Meier-Stiegen F, Fehm T, et al. Dormancy in breast cancer. Breast Cancer 2012;4:183–91.
3. Sosa MS, Bragado P, Aguirre-Ghiso JA. Mechanisms of disseminated cancer cell dormancy: an awakening field. Nat Rev Cancer 2014;14:611–22.
4. Yu M, Bardia A, Wittner BS, Stott SL, Smas ME, Ting DT, et al. Circulating breast tumor cells exhibit dynamic changes in epithelial and mesenchymal composition. Science 2013;339:580–4.
5. Broersen LH, van Pelt GW, Tollenaar RA, Mesker WE. Clinical application of circulating tumor cells in breast cancer. Cell Oncol 2014;37:9–15.
6. Banys M, Krawczyk N, Fehm T. The role and clinical relevance of disseminated tumor cells in breast cancer. Cancers 2014;6:143–52.
7. Ottewell PD, O'Donnell L, Holen I. Molecular alterations that drive breast cancer metastasis to bone. Bonekey Rep 2015;4:643.
8. Kim RS, Avivar-Valderas A, Estrada Y, Bragado P, Sosa MS, Aguirre-Ghiso JA, et al. Dormancy signatures and metastasis in estrogen receptor positive and negative breast cancer. PLoS One 2012;7:e35569.
9. Chen YC, Sosnoski DM, Mastro AM. Breast cancer metastasis to the bone: mechanisms of bone loss. Breast Cancer Res 2010;12:215.
10. Sosa MS, Avivar-Valderas A, Bragado P, Wen HC, Aguirre-Ghiso JA. ERK1/2 and p38α/β signaling in tumor cell quiescence: opportunities to control dormant residual disease. Clin Cancer Res 2011;17:5850–7.
11. Ghajar CM, Peinado H, Mori H, Matei IR, Evason KJ, Brazier H, et al. The perivascular niche regulates breast tumour dormancy. Nat Cell Biol 2013;15:807–17.
12. Wang N, Docherty F, Brown HK, Reeves K, Fowles A, Lawson M, et al. Mitotic quiescence, but not unique "stemness," marks the phenotype of bone metastasis-initiating cells in prostate cancer. FASEB J 2015;29:3141–50.
13. Patel P, Chen EI. Cancer stem cells, tumor dormancy, and metastasis. Front Endocrinol 2012;3:125.
14. Ogba N, Manning NG, Bliesner BS, Ambler SK, Haughian JM, Pinto MP, et al. Luminal breast cancer metastases and tumor arousal from dormancy are promoted by direct actions of estradiol and progesterone on the malignant cells. Breast Cancer Res 2014;16:489.
15. Lawson DA, Bhakta NR, Kessenbrock K, Prummel KD, Yu Y, Takai K, et al. Single-cell analysis reveals a stem-cell program in human metastatic breast cancer cells. Nature 2015;526:131–5.
16. Gao H, Chakraborty G, Lee-Lim AP, Mavrakis KJ, Wendel HG, Giancotti FG. Forward genetic screens in mice uncover mediators and suppressors of metastatic reactivation. Proc Natl Acad Sci U S A 2014;111:16532–7.
17. Sosa MS, Parikh F, Maia AG, Estrada Y, Bosch A, Bragado P, et al. NR2F1 controls tumour cell dormancy via SOX9- and RARbeta-driven quiescence programmes. Nat Commun 2015;6:6170.
18. Marlow R, Honeth G, Lombardi S, Cariati M, Hessey S, Pipili A, et al. A novel model of dormancy for bone metastatic breast cancer cells. Cancer Res 2013;73:6886–99.
19. Adam AP, George A, Schewe D, Bragado P, Iglesias BV, Ranganathan AC, et al. Computational identification of a p38SAPK-regulated transcription factor network required for tumor cell quiescence. Cancer Res 2009;69:5664–72.
20. Zhang H, Wang Y, Liu Z, Yao B, Dou C, Xu M, et al. Lymphocyte-specific protein 1 inhibits the growth of hepatocellular carcinoma by suppressing ERK1/2 phosphorylation. FEBS Open Bio 2016;6:1227–37.
21. Zhang XH, Jin X, Malladi S, Zou Y, Wen YH, Brogi E, et al. Selection of bone metastasis seeds by mesenchymal signals in the primary tumor stroma. Cell 2013;154:1060–73.
22. Su B, Zheng Q, Vaughan MM, Bu Y, Gelman IH. SSeCKS metastasis-suppressing activity in MatLyLu prostate cancer cells correlates with VEGF inhibition. Cancer Res 2006;66:5599–607.
23. Su B, Gao L, Baranowski C, Gillard B, Wang J, Ransom R, et al. A genome-wide RNAi screen identifies FOXO4 as a metastasis-suppressor through counteracting pi3k/akt signal pathway in prostate cancer. PLoS One 2014;9:e101411.
24. Akakura S, Nochajski P, Gao L, Sotomayor P, Matsui S, Gelman IH. Rb-dependent cellular senescence, multinucleation and susceptibility to oncogenic transformation through PKC scaffolding by SSeCKS/AKAP12. Cell Cycle 2010;9:4656–65.
25. Morgan M, Anders S, Lawrence M, Aboyoun P, Pages H, Gentleman R. ShortRead: a bioconductor package for input, quality assessment and exploration of high-throughput sequence data. Bioinformatics 2009;25:2607–8.

26. Zhang XH, Wang Q, Gerald W, Hudis CA, Norton L, Smid M, et al. Latent bone metastasis in breast cancer tied to Src-dependent survival signals. Cancer Cell 2009;16:67–78.
27. Aguirre-Ghiso JA, Bragado P, Sosa MS. Metastasis awakening: targeting dormant cancer. Nat Med 2013;19:276–7.
28. Muzes G, Sipos F. Metastatic cell dormancy and re-activation: an overview on series of molecular events critical for cancer relapse. Anticancer Agents Med Chem 2016;17:472–82.
29. Linde N, Fluegen G, Aguirre-Ghiso JA. The relationship between dormant cancer cells and their microenvironment. Adv Cancer Res 2016;132:45–71.
30. Brombin A, Joly JS, Jamen F. New tricks for an old dog: ribosome biogenesis contributes to stem cell homeostasis. Curr Opin Genet Dev 2015;34: 61–70.
31. Erol A, Acikgoz E, Guven U, Duzagac F, Turkkani A, Colcimen N, et al. Ribosome biogenesis mediates antitumor activity of flavopiridol in CD44 (+)/CD24(-) breast cancer stem cells. Oncol Lett 2017;14:6433–40.
32. Decker AM, Jung Y, Cackowski FC, Yumoto K, Wang J, Taichman RS. Sympathetic signaling reactivates quiescent disseminated prostate cancer cells in the bone marrow. Mol Cancer Res 2017;15:1644–55.
33. Myrvang HK, Guo X, Li C, Dekker LV. Protein interactions between surface annexin A2 and S100A10 mediate adhesion of breast cancer cells to microvascular endothelial cells. FEBS Lett 2013;587:3210–5.
34. Blancato J, Singh B, Liu A, Liao DJ, Dickson RB. Correlation of amplification and overexpression of the c-myc oncogene in high-grade breast cancer: FISH, in situ hybridisation and immunohistochemical analyses. Br J Cancer 2004;90:1612–9.
35. Bellovin DI, Das B, Felsher DW. Tumor dormancy, oncogene addiction, cellular senescence, and self-renewal programs. Adv Exp Med Biol 2013; 734:91–107.
36. Pohl SG, Brook N, Agostino M, Arfuso F, Kumar AP, Dharmarajan A. Wnt signaling in triple-negative breast cancer. Oncogenesis 2017;6:e310.
37. Asem MS, Buechler S, Wates RB, Miller DL, Stack MS. Wnt5a signaling in cancer. Cancers 2016;8:pii: E79.
38. Taciak B, Pruszynska I, Kiraga L, Bialasek M, Krol M. Wnt signaling pathway in development and cancer. J Physiol Pharmacol 2018;69:10.
39. Wawrzak D, Metioui M, Willems E, Hendrickx M, de GE, Leyns L. Wnt3a binds to several sFRPs in the nanomolar range. Biochem Biophys Res Commun 2007;357:1119–23.
40. Huelsken J. Tumor-stroma crosstalk via Hedgehog and Wnt pathways bypasses resident immune cells to enable liver metastases. Cancer Res 2016;76. Available from: https://www.aacr.org/Meetings/Pages/Program-Detail.aspx?EventItemID=55&DetailItemID=299&Day=12012015.
41. Radvanyi L, Singh-Sandhu D, Gallichan S, Lovitt C, Pedyczak A, Mallo G, et al. The gene associated with trichorhinophalangeal syndrome in humans is overexpressed in breast cancer. Proc Natl Acad Sci U S A 2005;102: 11005–10.
42. Curtis C, Shah SP, Chin SF, Turashvili G, Rueda OM, Dunning MJ, et al. The genomic and transcriptomic architecture of 2,000 breast tumours reveals novel subgroups. Nature 2012;486:346–52.
43. Pereira B, Chin SF, Rueda OM, Vollan HK, Provenzano E, Bardwell HA, et al. The somatic mutation profiles of 2,433 breast cancers refines their genomic and transcriptomic landscapes. Nat Commun 2016;7:11479.
44. Curigliano G, Goldhirsch A. The triple-negative subtype: new ideas for the poorest prognosis breast cancer. J Natl Cancer Inst Monogr 2011;2011: 108–10.
45. Nandana S, Tripathi M, Duan P, Chu CY, Mishra R, Liu C, et al. Bone metastasis of prostate cancer can be therapeutically targeted at the TBX2-WNT signaling axis. Cancer Res 2017;77:1331–44.
46. Asanoma K, Liu G, Yamane T, Miyanari Y, Takao T, Yagi H, et al. Regulation of the mechanism of TWIST1 transcription by BHLHE40 and BHLHE41 in cancer cells. Mol Cell Biol 2015;35:4096–109.
47. Adorno M, Cordenonsi M, Montagner M, Dupont S, Wong C, Hann B, et al. A mutant-p53/Smad complex opposes p63 to empower TGFbeta-induced metastasis. Cell 2009;137:87–98.
48. Piccolo S, Enzo E, Montagner M. p63, Sharp1, and HIFs: master regulators of metastasis in triple-negative breast cancer. Cancer Res 2013;73:4978–81.
49. Chen H, Liu H, Qing G. Targeting oncogenic Myc as a strategy for cancer treatment. Signal Transduct Target Ther 2018;3:5.
50. Yee-Lin V, Pooi-Fong W, Soo-Beng AK. Nutlin-3, A p53-Mdm2 antagonist for nasopharyngeal carcinoma treatment. Mini Rev Med Chem 2018;18: 173–83.
51. Zheng S, Liu J, Wu Y, Huang TL, Wang G. Small-molecule inhibitors of Wnt signaling pathway: towards novel anticancer therapeutics. Future Med Chem 2015;7:2485–505.
52. Lee HJ, Bao J, Miller A, Zhang C, Wu J, Baday YC, et al. Structure-based discovery of novel small molecule wnt signaling inhibitors by targeting the cysteine-rich domain of frizzled. J Biol Chem 2015;290:30596–606.
53. Igea A, Nebreda AR. The stress kinase p38alpha as a target for cancer therapy. Cancer Res 2015;75:3997–4002.